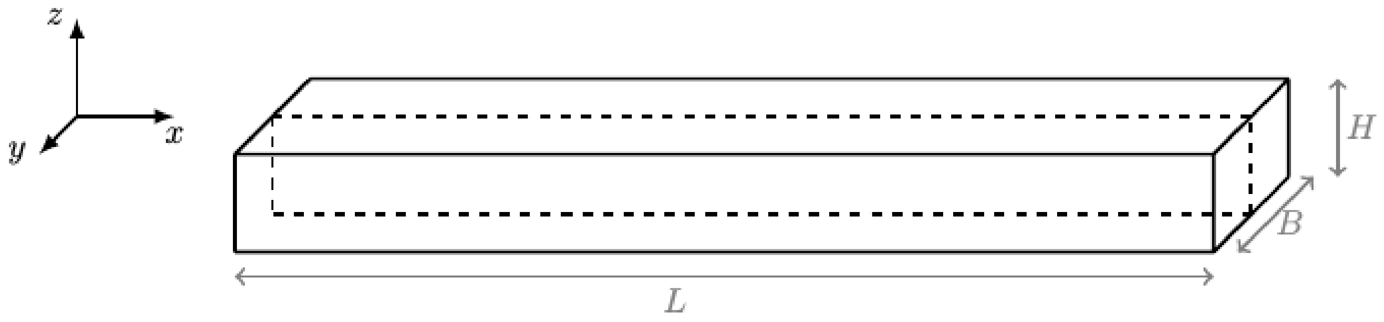

Flanders
State of the Art

19_025_2
FHR reports

Study of a simplified Scheldt model

Sub report 2
comparison between iFlow and Telemac

DEPARTMENT
MOBILITY &
PUBLIC
WORKS

www.flandershydraulicsresearch.be

Study of a simplified Scheldt model

Subreport 2: comparison between iFlow and Telemac

Kaptein, S.J.; Bi, Q.; Schramkowski, G.; Mostaert, F.

Flanders
Hydraulics Research

Flanders
State of the Art

Cover figure © The Government of Flanders, Department of Mobility and Public Works, Flanders Hydraulics Research

Legal notice

Copyright and citation

D/2020/3241/194

This publication should be cited as follows:

Kaptein, S.J.; Bi, Q.; Schramkowski, G.; Mostaert, F. (2020). Study of a simplified Scheldt model: Subreport 2: comparison between iFlow and Telemac. Version 2.0. FHR Reports, 19_025_2. Flanders Hydraulics Research: Antwerp

Document identification

Customer:	Flanders Hydraulics Research		Ref.:	WL2020R19_025_2
Keywords (3-5):	Idealized modelling, numerical simulations, Scheldt			
Knowledge domains:	Hydraulics and sediment > Tides > Numerical modelling - Hydraulics and sediment > Water levels > Numerical modelling			
Text (p.):	18		Appendices (p.):	0
Confidentiality:	No	☒ Available online		

Author(s):	Kaptein, S.J.; Bi, Q.

Control

	Name	Signature
Revisor(s):	Schramkowski, G.	Dr. George P. Schramkowski Digitaal ondertekend door Dr. George P. Schramkowski Datum: 2020.11.26 12:49:59 +01'00'
Project leader:	Kaptein, S.J.	Getekend door: Steven Kaptein (Signature) Getekend op: 2020-11-30 10:45:19 +00:00 Reden: Ik keur dit document goed Steven Kaptein

Approval

Head of division:	Mostaert, F.	Getekend door: Frank Mostaert (Signature) Getekend op: 2020-11-27 09:49:06 +00:00 Reden: Ik keur dit document goed Frank Mostaert

Abstract

The objective of this report is to compare the results of two different modeling tools iFlow and Telemac. Each modeling tool is applied to an extremely simplified Scheldt model: a geometry with a rectangular cross-section, a constant width and a constant depth. The main purpose of the study is to challenge the assumptions on which iFlow is based and to estimate the extend to which they influence the reliability of the results. The results show that it was not possible to determine a ratio of between the water depth and the amplitude of the M2 tide for which iFlow clearly fails to reproduce the results of Telemac, in the present flow configuration and for the present parameters. Additionally, no single parameter governing the differences between iFlow and Telemac has been identified. However, more data (i.e. number of simulations) is required to carry out a significant study about the differences between iFlow and Telemac and iFlow needs to be pushed to the limits in terms of the ratio between the water depth and the magnitude of the M2 tide.

Contents

List of Figures

List of Tables

1 Introduction

The use of complex three-dimensional models, such as Telemac, for studying estuaries has been a common practice over the last decades (Malcherek, 2000; Smolders *et al.*, 2016). Their accurate implementation of the river geometry, the river bathymetry, the external forcing and the possibility of including tributaries or coastal regions make them an appreciated tool for investigating case studies. However, two of the major drawbacks of complex three-dimensional models are (i) their lack of short computational time and (ii) the complex analysis of the results. These features make it almost impossible to investigate more than one or two scenarios or to give an interpretation of the results based on individual physical processes.

Subsequently, the use of faster, idealized and process based models, such as iFlow, have become more and more popular over the last years (Brouwer *et al.*, 2018; Brouwer *et al.*, 2017; Dijkstra *et al.*, 2017, 2019a,b). These models allow for the simulation of multiple scenarios (e.g. order of magnitude hundred to thousand) at reasonable computational costs. Additionally, the way iFlow is constructed allows for a decomposition of the different variables (i.e. water-level, velocity fields, sediment concentrations) into the sum of individual contributions. Each of these contributions corresponds then to a specific physical mechanism. A major drawback is that iFlow uses a highly idealized representation of an estuary. For example, the bathymetry is smoothened and the model is width-averaged. Some of the fundamental simplifying assumptions are not necessarily met (more detail about these assumptions in Section 2).

In order to solve the drawbacks of each of the two models, a comparison is undertaken. This comparison will clarify the influence of some of the simplifying assumptions on iFlow's results. While iFlow and Telemac are based on similar sets of equations, they adopt distinctive boundary conditions and fundamlentally different solution methods. Accordingly, rigorous choices are required and need to be motivated in order to bring iFlow and Telemac as close together as possible. These choices include the grid properties, model parameters and boundary conditions, and are detailed in Sections 2, 3 and 4. To identify and limit the number of discrepancies of the model, it was chosen to gradually increase the complexity of the study case by starting from the most simple case: a semi-enclosed rectilinear tidal channel of rectangular cross-section, with a constant depth and width, and forced at one end by an M2 and an M4 signal.

2 The iFlow model

2.1 Governing equations

The iFlow model solves the **width-averaged** Saint-Venant (or shallow water) equations for the conservation of momentum, as well as a **width-averaged** continuity equation for the conservation of mass

$$\frac{\partial u}{\partial t} + u\frac{\partial u}{\partial x} + w\frac{\partial u}{\partial z} = -g\frac{\partial \zeta}{\partial x} - \int_{z}^{R+\zeta} \frac{1}{\rho_{\text{ref}}}\frac{\partial \rho}{\partial x} d\tilde{z} + \frac{\partial}{\partial z}\left(\nu_{T}\frac{\partial u}{\partial z}\right), \tag{1a}$$

$$B\frac{\partial w}{\partial z} + \frac{\partial Bu}{\partial x} = 0, \tag{1b}$$

in which u and w are the velocity variables, respectively along x (along estuary coordinate), and along z (vertical coordinate). The symbol t represents time, g the acceleration of gravity, ζ the surface elevation, R the mean level of the river surface, ρ_{ref} the reference density, ρ the density of the fluid, ν_T the eddy-viscosity, H the water depth and B the channel width.

The associated boundary conditions comprise a partial slip condition and a no-penetration condition at the bed (i.e. $z = -H$), a no-stress condition and a kinematic boundary condition at the surface (i.e. $z = R + \zeta$), a time-dependent tidal forcing at the seaward boundary (i.e. $x = 0$) and an imposed river discharge at the landward boundary (i.e. $x = L$). The equations for these boundary conditions are

$$\nu_T\frac{\partial u}{\partial z} = s_f u \qquad \text{at } z = -H, \tag{2a}$$

$$w + u\frac{\partial H}{\partial x} = 0 \qquad \text{at } z = -H, \tag{2b}$$

$$\nu_T\frac{\partial u}{\partial z} = 0 \qquad \text{at } z = R + \zeta, \tag{2c}$$

$$w = \frac{\partial \zeta}{\partial t} + u\frac{\partial \zeta}{\partial x} \qquad \text{at } z = R + \zeta, \tag{2d}$$

$$\zeta = A_{\text{M}_2}\cos(\sigma t) + A_{\text{M}_4}\cos(2\sigma t + \varphi) \qquad \text{at } x = 0, \tag{2e}$$

$$B\int_{-H}^{R+\zeta} u dz = -Q \qquad \text{at } x = L. \tag{2f}$$

Several new parameters appear: s_f, the friction coefficient, A_{M_2} and σ, respectively the amplitude and the frequency of the M$_2$ tide, A_{M_4}, the amplitude of the M$_4$ tide, and Q the river discharge, and φ the phase of the M$_4$ tide.

It is possible to derive an equation for the surface elevation by integrating Eq. (1b) over the depth and to use Eqs (2b) and (2d),

$$B\frac{\partial \zeta}{\partial t} + \frac{\partial}{\partial x}\left(B\int_{-H}^{R+\zeta} u dz\right) = 0 \tag{3}$$

2.2 Resolution techniques

The resolution technique for solving Eqs (1a), (3) relies on the linearization of the equations. By making the equations non-dimensional using L for x, H for the z, A_{M_2} for ζ and σ for t, it is possible to show that the non-linear advection terms scale with $\varepsilon = A_{\text{M}_2}/H$ (see Brouwer *et al.*, 2017 for more details). If we assume that the baroclinic term also scales with ε and that $\varepsilon \ll 1$, the solution can take the form of a series in which the variables are decomposed as

$$
\begin{aligned}
u &= u_0 + u_1 + u_2 + \cdots, \\
w &= w_0 + w_1 + w_2 + \cdots, \\
\zeta &= \zeta_0 + \zeta_1 + \zeta_2 + \cdots
\end{aligned}
$$

with $u_1/u_0 \sim \varepsilon$, $u_2/u_1 \sim \varepsilon$ and $\varepsilon \ll 1$ (and similarly for w and ζ). Accordingly, it is possible to split the governing equations and the associated boundary conditions into a set of equations governing the leading order variables and a set of equations governing the first order variables. At leading order, this decomposition gives

$$
\frac{\partial u_0}{\partial t} - \frac{\partial}{\partial z}\left(\nu_T \frac{\partial u_0}{\partial z}\right) = -g\frac{\partial \zeta_0}{\partial x}, \tag{4a}
$$

$$
B\frac{\partial \zeta_0}{\partial t} + \frac{\partial}{\partial x}\left(B\int_{-H}^{R} u_0 dz\right) = 0, \tag{4b}
$$

$$
B\frac{\partial w_0}{\partial z} + \frac{\partial B u_0}{\partial x} = 0, \tag{4c}
$$

for the governing equations, and

$$
\begin{aligned}
\nu_T \frac{\partial u_0}{\partial z} &= s_f u_0 && \text{at } z = -H, && (5a)\\
w_0 + u_0 \frac{\partial H}{\partial x} &= 0 && \text{at } z = -H, && (5b)\\
\nu_T \frac{\partial u_0}{\partial z} &= 0 && \text{at } z = R, && (5c)\\
\zeta_0 &= A_{\text{M}_2}\cos(\sigma t) && \text{at } x = 0, && (5d)\\
B\int_{-H}^{R} u_0 dz &= 0 && \text{at } x = L, && (5e)
\end{aligned}
$$

for the boundary conditions.

At first order the decomposition leads to

$$
\frac{\partial u_1}{\partial t} - \frac{\partial}{\partial z}\left(\nu_T \frac{\partial u_1}{\partial z}\right) = -\, g\frac{\partial \zeta_1}{\partial x} - \int_{z}^{R} \frac{1}{\rho_{\text{ref}}}\frac{\partial \rho_0}{\partial x} d\tilde{z} - u_0\frac{\partial u_0}{\partial x} - w_0\frac{\partial u_0}{\partial z}, \tag{6a}
$$

$$
B\frac{\partial \zeta_1}{\partial t} = -\frac{\partial}{\partial x}\left(B\int_{-H}^{R} u_1 dz\right) - \frac{\partial}{\partial x}\left(B\, u_0|_R\, \zeta_0\right), \tag{6b}
$$

$$
B\frac{\partial w_1}{\partial z} = -\frac{\partial B u_1}{\partial x}, \tag{6c}
$$

for the governing equations, and

$$\nu_T \frac{\partial u_1}{\partial z} = s_f u_1 \qquad \text{at } z = -H, \tag{7a}$$

$$w_1 + u_1 \frac{\partial H}{\partial x} = 0 \qquad \text{at } z = -H, \tag{7b}$$

$$\nu_T \frac{\partial u_1}{\partial z} = -\zeta_0 \frac{\partial}{\partial z}\left(\nu_T \frac{\partial u_0}{\partial z}\right) \qquad \text{at } z = R, \tag{7c}$$

$$\zeta_1 = A_{\text{M}_4} \cos(2\sigma t + \varphi) \qquad \text{at } x = 0, \tag{7d}$$

$$\int_{-H}^{R} u_1 dz = -\frac{Q_1}{B} - u_0|_R \; \zeta_0 \qquad \text{at } x = L, \tag{7e}$$

for the boundary conditions.

As mentioned previously, this decomposition linearizes the equations. Subsequently, superposition techniques can be applied (i.e. solution of the sum is equal to the sum of the solution). It is this technique that allows to consider different forcing mechanism independently of the others.

The last characteristic **assumption of iFlow is the harmonic decomposition**. The harmonic decomposition implies that only the steady state solution is solved and that:

$$\frac{\partial \hat{u}_0}{\partial t} = \mathrm{i}\sigma \hat{u}_0$$
$$\frac{\partial \hat{u}_1}{\partial t} = 2\mathrm{i}\sigma \hat{u}_1$$

with $\hat{u}$ the complex velocity associated to u. The same decomposition applies to w and ζ. As a result, the leading order variables evolve with the M2 tidal frequency while the first order variable evolve with the M4 tidal frequency but also have a residual component. Depending on the numerical settings, iFlow can solve the first and leading order equations (semi-)analytically or numerically. For more information about the solving procedures, the reader is referred to the literature (Dijkstra, 2017; Dijkstra *et al.*, 2017).

To summarize, the **three major assumption of iFlow that are not** necessarily present in Telemac are

1. the tidal amplitude is much smaller than the water depth
2. the baroclinic term only appears at first order (weak horizontal density gradient)
3. the time evolution is periodic with harmonic equal to the M2 tidal frequency and the M4 tidal frequency

In the present report, we will focus on assumption 1 by performing 27 different simulations, each with a different depth. In each simulation the amplitude of the M2 and M4 amplitude are kept small, such that a difference in water depth results immediately in a different ratio between tidal amplitude and the constant water-depth. Simultaneously, any standard error not related to this ratio could also challenge assumption 3. It is important to not that the standard bottom boundary condition implemented in Telemac is a quadratic friction law. However, in order to have consistency between iFlow and Telemac, the linear friction law of iFlow has been implemented in Telemac.

3 The Telemac model

3.1 Governing equations

This section is entirely taken over from Bi et al.*, 2020*

The hydrodynamics in Telemac-3D is modeled with 3D incompressible Reynolds-averaged Navier-Stokes equations. The Navier–Stokes equations for incompressible flows consist of two equations: the continuity and the momentum equations. Assuming that fluid density is incompressible, and applying the Boussinesq approximation to the Reynolds stress term, the mass and momentum conservation equations under vector form read:

$$\nabla \cdot \mathbf{u} = 0 \tag{8}$$

$$\frac{\partial \mathbf{u}}{\partial t} + (\mathbf{u} \cdot \nabla)\mathbf{u} = -\frac{1}{\rho}\nabla p + \nabla \cdot [(\nu + \nu_T)\,\nabla \mathbf{u}] + \mathbf{g} + \mathbf{F} \tag{9}$$

where ∇ is the gradient operator, **u** is the Reynolds-averaged mean velocity vector, t is the time, ρ is the fluid density, p is the mean pressure, ν is the kinematic viscosity of the fluid, ν_T is the turbulence eddy viscosity, **g** is the gravitational force vector and **F** is the vector containing other external forces, e.g. Coriolis force and centrifugal force. In many industrial and environmental flows, the density of the carrying phase is not a constant but varies as a function of the temperature, salinity and/or sediment concentration. The buoyancy effects due to the density gradient thus should be included in the governing equations in order to model the stratification properly. The varying density could be included in the Eq. (8) and Eq. (9). But there is also an alternative way that enables the treatment of buoyancy effect by means of the gravity term if the change of density $\Delta\rho/\rho < 0.1)$. Based on this assumption, an extra term representing the buoyancy force can be derived and added into the momentum equation. The details can be found in the Telemac-3D theory guide. To the governing equations, the turbulence eddy viscosity ν_T has to be closed with a turbulence model. However, in this project, the eddy-viscosity was taken constant.

3.2 Bottom boundary condition

One of the major differences between iFlow and Telemac resides in the bottom boundary condition. First iFlow assumes a partial slip condition with a linear formulation of the velocity dependence of the stresses at the bottom. Telemac uses a quadratic formulation. Second, in iFlow, the boundary condition is really applied at the bottom, while in Telemac the boundary condition is applied at the center of the first cell above the bottom. If we note Δz the distance of the first cell center from the bottom wall, the application of a partial slip boundary condition is formulated as

$$\nu_T \frac{\partial u}{\partial z} = s_f u \qquad \text{at } z = -H + \Delta z. \tag{10}$$

Using a Taylor series development of Eq. (10) at $z = -H + \Delta z$ gives

$$\nu_T \frac{\partial u}{\partial z} + \Delta z \frac{\partial}{\partial z}\left(\nu_T \frac{\partial u}{\partial z}\right) = s_f u + \Delta z \frac{\partial}{\partial z}\left(s_f u\right) + O\left(\Delta z^2\right) \qquad \text{at } z = -H + \Delta z, \tag{11}$$

which is different from the formulation in iFlow (see Eq. (2a)). In other words, applying the partial slip boundary at $z = -H + \Delta z$ instead of $z = -H$ gives an error of

$$\Delta z \frac{\partial}{\partial z}\left(s_f u - \left(\nu_T \frac{\partial u}{\partial z}\right)\right), \tag{12}$$

which can be controlled by refining the grid close to the bottom boundary.

4 Simulation set-up

4.1 Computational domain and grid

As mentioned in the earlier sections, the model is kept as simple as possible in the first instance before being complexified gradually. We start with a semi-enclosed rectilinear channel of constant rectangular cross-section for the idealized Scheldt geometry. This set-up is sketched in Fig. 1 by the solid lines. Since iFlow is width-averaged, i.e. two-dimensional-vertical, the computation domain is rectangular and sketched by the dashed lines.

Figure 1 – Sketch of the computational domain for the Scheldt model, simplified to a maximum.

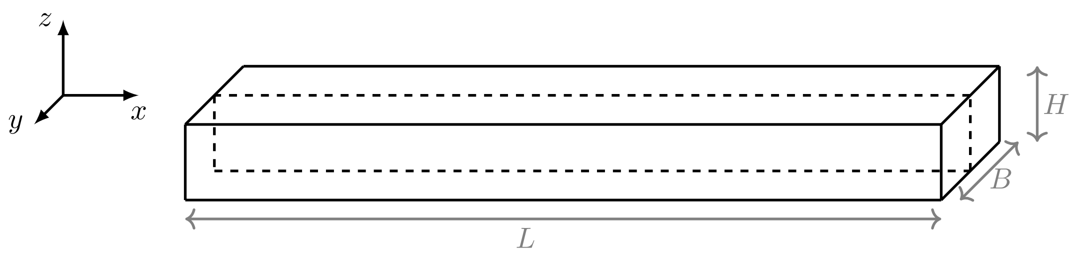

Since iFlow is a width-averaged model and Telemac not, different choices are possible for the horizontal grid-cell distribution in Telemac. We choose a regular triangulated grid as displayed in Fig 2.

Figure 2 – Grid configuration near the seaward boundary.

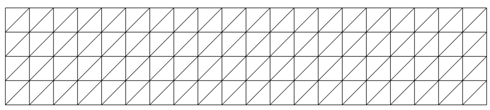

4.2 Simulation settings

The settings used in the different simulations are summarized in Table 1. In this table the phase of the M4 tide at $x = 0$, i.e. φ_{M_h} is also given.

Table 1 – Parameter values for an idealized Scheldt model

L (km)	B (m)	A_{M_2} (m)	A_{M_4} (m)	φ_{M_h} (rad)	Q1 (m^3 s^{-1})	ν_T (m^2 s^{-1})	s_f (m^3 s^{-1})
160	500	1.0	0.1	0	36	0.0367	0.0048

5 Results

5.1 Post-processing of the Telemac simulations

Since iFlow and Telemac differ in their method of solving the governing equations, some post-processing is required before comparing the results. On the one hand, iFlow provides the water level, and the velocities under the form of an M2 and an M4 signal, each characterized by an amplitude and a phase as a function of the x position (and the z position for the depth). On the other hand, Telemac provides the instantaneous value of the water level and the velocity over the entire domain, at specific time steps. It was chosen to extract the M2 signals M4 from the Telemac data to perform a direct comparison with the iFlow output. This extraction requires a specific protocol:

- At each grid point, a time-series of the water-level and the velocity is recorded.
- For each time-series, a specific M2 tidal period is selected that is not influenced by the spin-up of the simulation.
- The data available for this period is interpolated on an equidistant temporal grid, in such a way that one period contains exactly an integer number of time-steps.
- A fast Fourrier transform is applied to the interpolated data which gives the amplitudes and phases for M2, M4 and higher order frequencies.
- Finally, a spatial distribution of the amplitudes and phases for the different frequencies is reconstructed.

In this protocol, the size of the Telemac data (several Gb) caused the initial scripts to be very time consuming (several hours to process one simulation). Accordingly, some time was allocated (and spent) in order to optimize the scripts. They currently run in a couple of tens of seconds. A second challenge that emerged, was the estimation of the convergence time in Telemac. It was chosen to simulated 40 days (approximately 75 tidal periods), which took between 6 to 7 hours on a laptop.

5.2 Convergence of the Telemac simulations

In practice, it was found that convergence was not reached within the 40 days simulation time for all the configurations tested. To backup-up this statement, it is important to clarify the convergence criteria. It is assumed that convergence is reached locally when the relative error η_ψ, locally defined as,

$$\eta_\psi(x) = \left| \frac{\psi_i(x) - \psi_{i+1}(x)}{\psi(x)} \right| \tag{13}$$

is smaller than at least ε^2 all over the estuary. Arbitrary, we set then maximum tolerated relative error to 10^{-3}. In Eq. (13), ψ refers to a quantity such as a time-series, the amplitude along the estuary or the phase along the estuary. The subscript i refers to a specific period. The threshold value of 10^{-3} might seem very small. However, to carry out a meaningful comparison, the error due to the lack of convergence needs to be negligible with respect to the relative difference between iFlow results and Telemac results.

Simulating 40 days (or 75 tidal periods) in Telemac on one processor took between 6 or 7 hours (wall time). As a result, a crucial step in this protocol is to determine the number of periods after which the simulation is converged. Ideally, as few periods as possible should be simulated in order reduce significantly computation time and stored data. However, the number of periods is difficult to estimate since the number of periods after which convergence is obtained varies considerably with the set-up. This phenomenon is illustrated in Figs 3 and 4, by means of the relative error ε_ψ and the absolute error, $\eta_{\psi_a}(x) = |\psi_i(x) - \psi_{i+1}(x)|$. For a ratio $h/A_{\mathrm{M_2}} = 20$ (Fig. 3), the absolute difference in M2 tide amplitude between two successive periods is of the order of 10^{-7}m over the estuary. The relative difference is of order 1.0×10^{-7}%. These results indicate a satisfying convergence.

Figure 3 – Magnitude of the M2 tide over the estuary computed for two different period numbers (left). Difference and relative difference between these two signals (right). The two chosen periods are the last period and the second last period of a 40 day simulation. Simulation for $h = 20$m and $A_{\mathrm{M_2}} = 1$m.

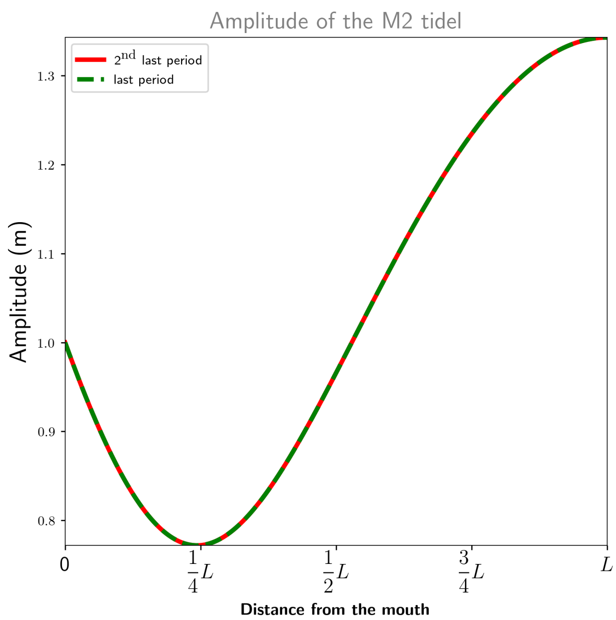

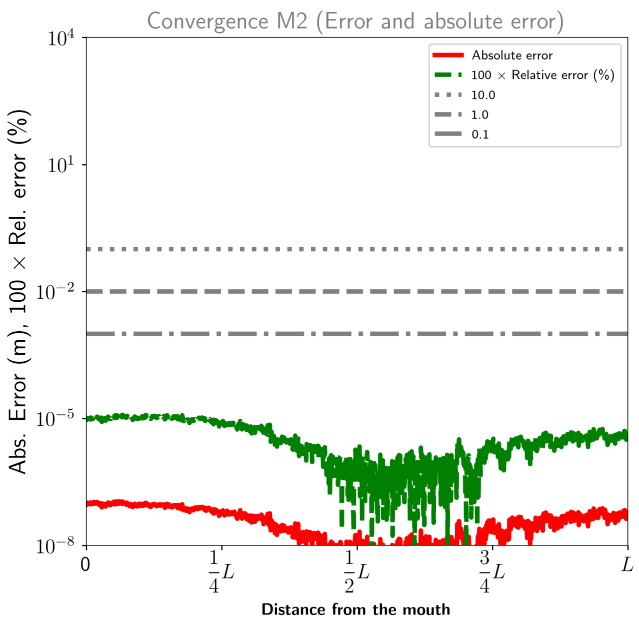

In contrast, for a ratio $h/A_{\mathrm{M_2}} = 3$ (Fig. 4), the relative difference if M2 tide amplitude between two successive periods is almost of order 10% towards the landwards side of the estuary. Nevertheless, the absolute error is still of order 10^{-7}m. Additionally, the amplitude in the M2 tidal signal is very small towards the landward side of the estuary. These two observations indicate that the small tidal amplitude provokes a slow convergence of the relative error in the M2 tidal signal, such that a longer simulation period might be required for a simulation with $h/A_{\mathrm{M}_2} = 3$ in the present configuration.

Figure 4 – Magnitude of the M2 tide over the estuary computed for two different period numbers (left). Difference and relative difference between these two signals (right). The two chosen periods are the last period and the second last period of a 40 day simulation. Simulation for $h = 3$m and $A_{\mathrm{M}_2} = 1$m.

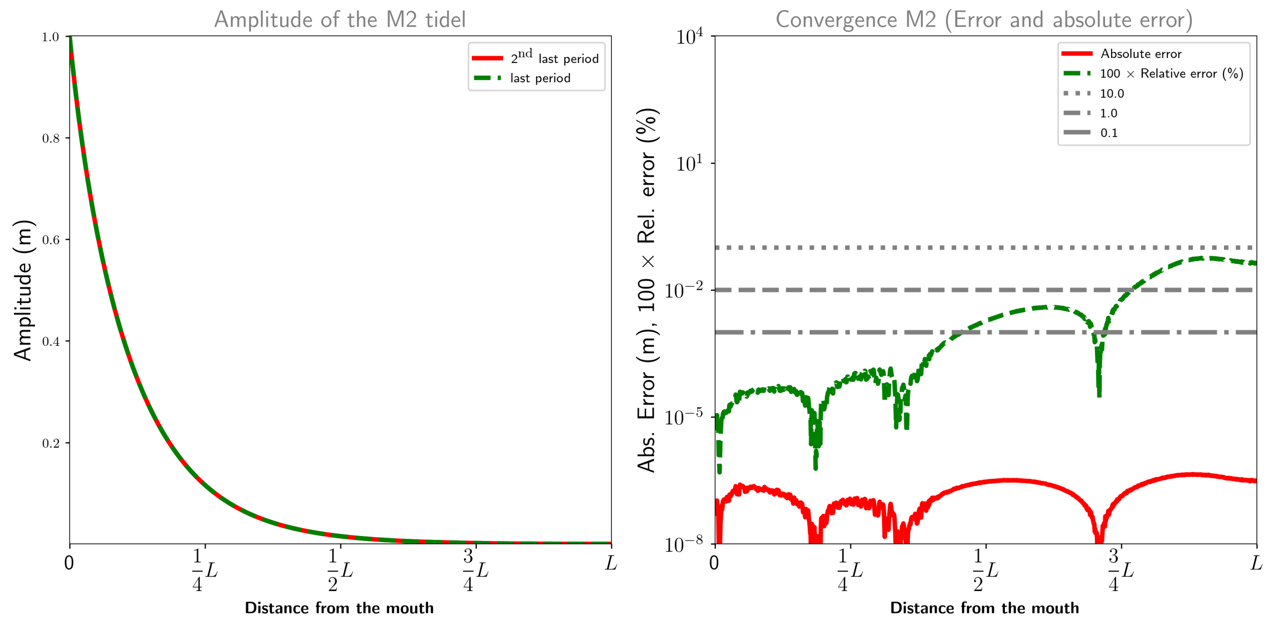

To compare the convergence rate in between the simulations, we define a norm $N_{\eta,\psi}$ by averaging the error η_ψ over the estuary according to

$$N_{\varepsilon,\psi} = \frac{1}{L}\int_0^L \eta_\psi(x)dx. \tag{14}$$

In Eq. (14), the norm operator is applied to the relative error, but the norm for the absolute error is defined by the same operator. The order of magnitude of $N_{\eta,|\zeta_0|}$ and $N_{\eta,|\zeta_1|}$ for the convergence is shown in Fig 5 for different values of h/A_{M_2}. From this figures, it appears that: (i) the absolute error is of order 10^{-7}m for all the tested values of h/A_{M_2}, and for the both the M2 signal and the M4 signal; (ii) the relative error is approximately one order of magnitude larger for the M4 signal than for the M2 signal (which makes sence since the relative error is normalized by the tidal signal and the M4 tidal signal has a smaller amplitude than the M2 tidal signal); (iii) the simulation with $h/A_{\mathrm{M}_2} = 3$ is only with a significantly larger magnitude of the norm of the relative error, suggesting convergence was not reached yet. This latter observation is strange since a smaller depth means increased friction, thus a shorter time to reach the stationary solution.

Figure 5 – Convergence norm for simulations with different values of h/A_{M_2}, ranging from $h/A_{\mathrm{M}_2} = 3$ to $h/A_{\mathrm{M}_2} = 100$.

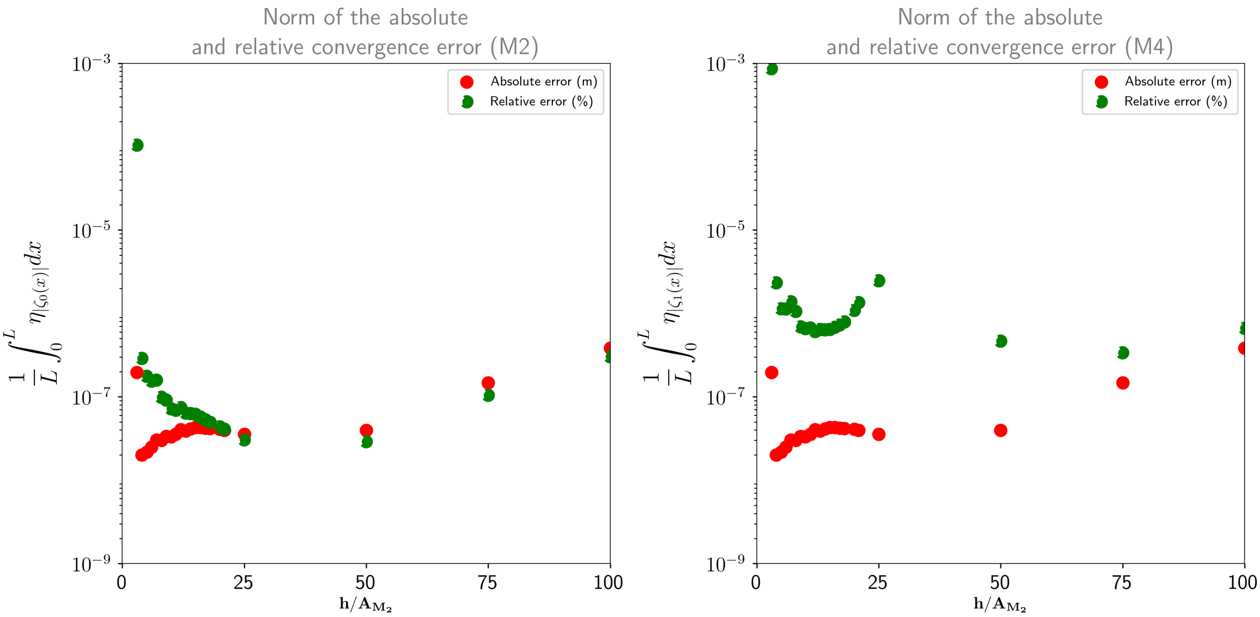

5.3 Comparison between iFlow and Telemac

The difference between the iFlow results and the Telemac results is shown in Figs 6 and 7 for two different values of the $h/A_{\mathrm{M_2}}$ ratio. Clearly, the amplitude and the phase of the M2 and the M4 tide overlap for $h/A_{\mathrm{M_2}}$=20 (see Fig. 6). However, for $h/A_{\mathrm{M_2}}$=3, some small descrepancies are noticible in the amplitudes and some more significant difference are observable in the phases (see Fig. 7).

Figure 6 – Difference between iFlow and Telemac results for a simulation with $h/A_{\mathrm{M_2}}$=20.

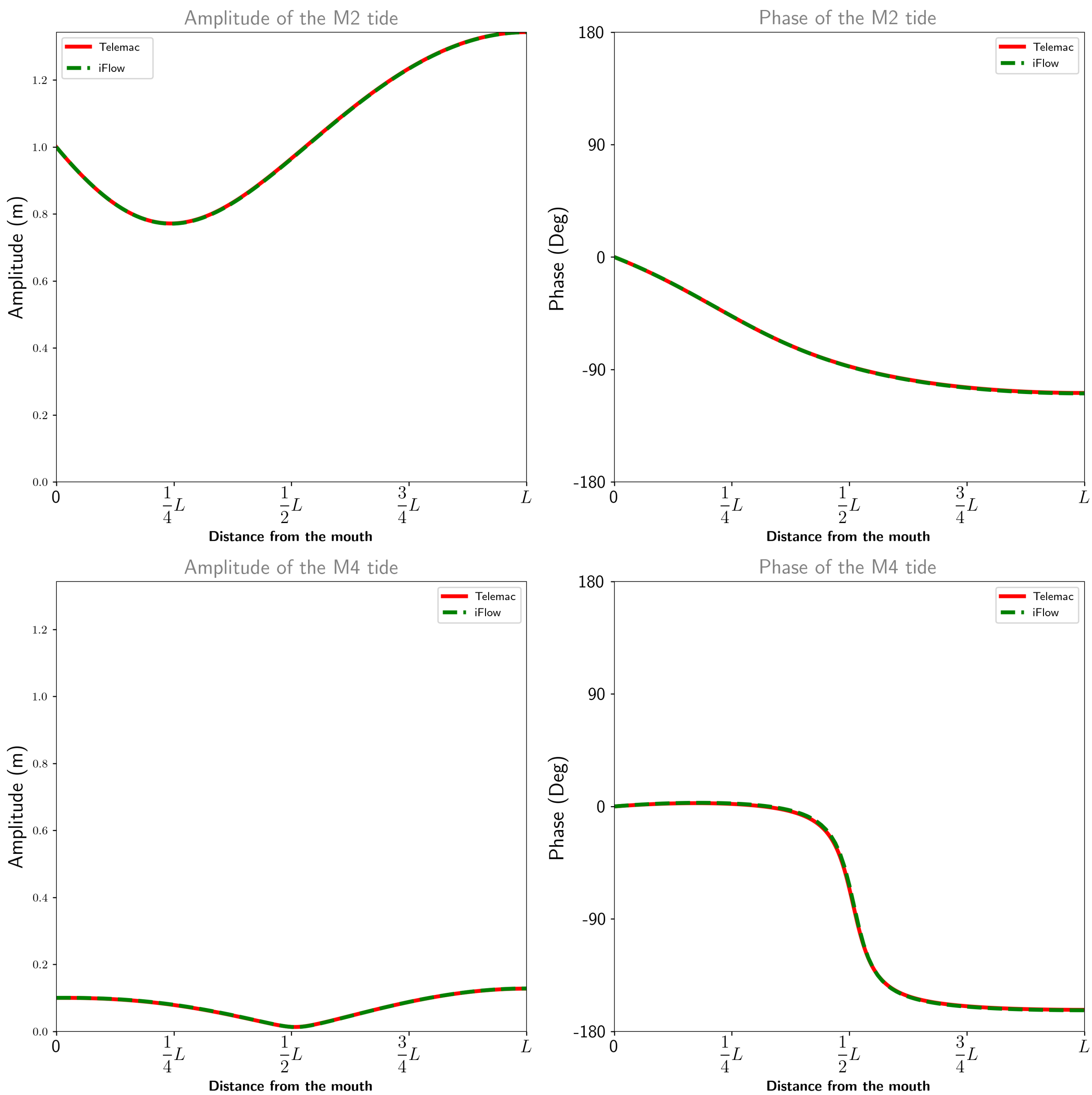

To estimate the influence of the ratio $h/A_{\mathrm{M_2}}$ on the difference between the results computed by iFlow and the results computed by Telemac, we introduce the relative difference E_ψ. This relative difference is analogous to

Figure 7 – Difference between iFlow and Telemac results for a simulation with $h/A_{\mathrm{M_2}}$=3.

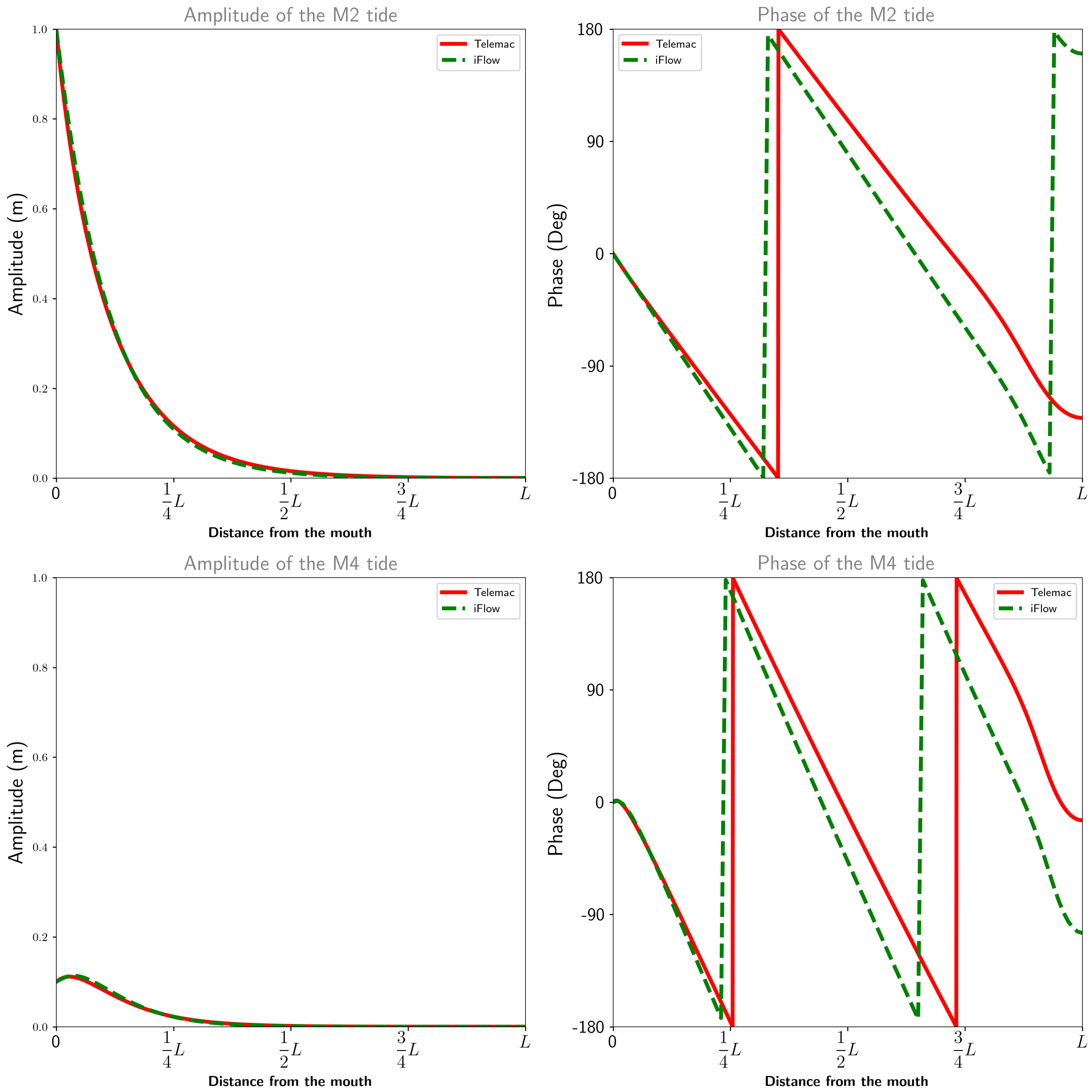

the relative error ε_ψ and is defined as

$$E_\psi(x) = \left| \frac{\psi_{Te}(x) - \psi_{iF}(x)}{\psi_{Te}(x)} \right|. \tag{15}$$

In Eq. (15), ψ still refers to a physical quantity. The absolute difference would be defined as, $E_{\psi_a}(x) = |\psi_{Te}(x) - \psi_{iF}(x)|$. Analogy with Eq. (14), we define the norm of the relative difference

$$N_{E,\psi} = \frac{1}{L} \int_0^L E_\psi(x) dx. \tag{16}$$

The norm of the absolute difference does not show a clear trend with $h/A_{\mathrm{M_2}}$ (see Fig. 8). Nevertheless, the norm of the relative difference is the highest for the low values of the $h/A_{\mathrm{M_2}}$ ratio, suggesting that for these values of h/A_{M_2}, the iFlow assumptions start to be challenged. However, these values also correspond to the simulations for which convergence is still disputed, although the values of $N_{\varepsilon,\psi}$ (measure of the convergence) are significantly smaller than the value for $N_{E,\psi}$ (measure of the difference).

Figure 8 – Difference norm for simulations with different values of h/A_{M_2}.

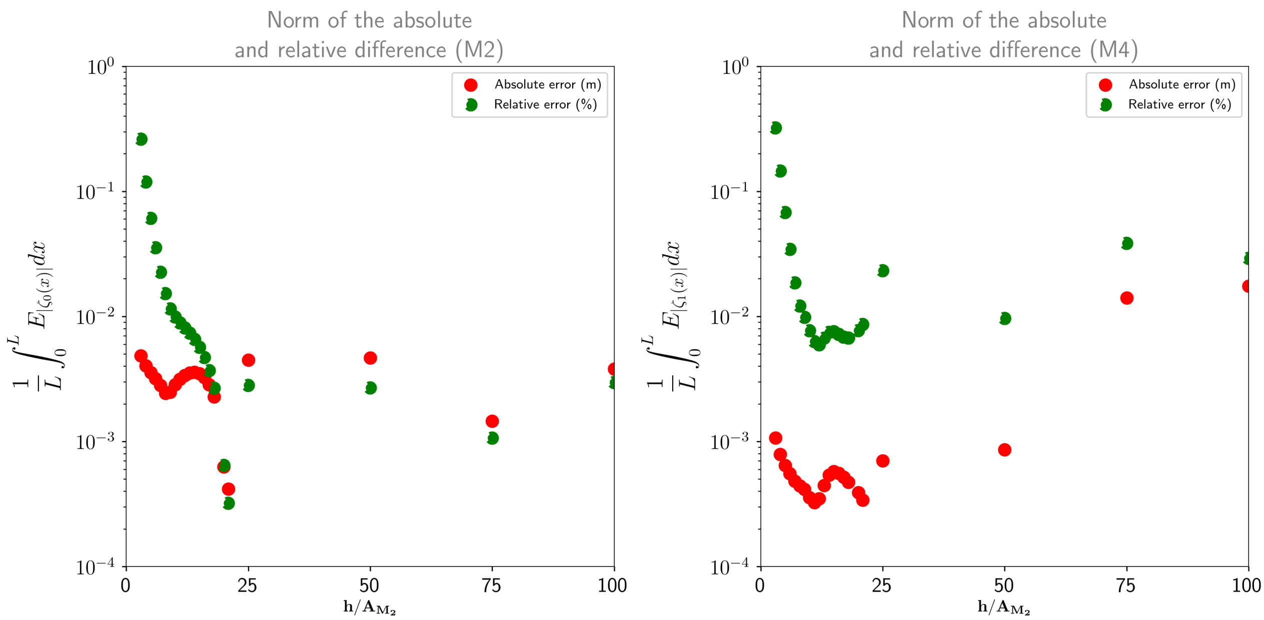

A peculiar feature of the evolution of the $N_{E,\psi}$ norm, is that there is no steady dependence on h/A_{M_2}. This phenomenon could be related to the quality of the h/A_{M_2} ratio as a measure for ε. Indeed, as can be seen in Figs 3 and 7, the damping of the tidal amplitude for h/A_{M_2} is relatively fast, which implies that the ε becomes very small in a relatively short distance from the mouth, even if it is large at the mouth itself.

5.4 Estuary averaged epsilon

To overcome the shortcoming of the ε criterion, it is possible to define an average ε, $\overline{\varepsilon}$ as

$$\overline{\varepsilon} = \frac{1}{L}\int_0^L \frac{A_{\mathrm{M}_2}(x)}{h(x)}dx \tag{17}$$

for h/M_2, and

$$\overline{\varepsilon} = \frac{1}{L}\int_0^L \frac{A_{\mathrm{M}_4}(x)}{A_{\mathrm{M}_2}(x)}dx \tag{18}$$

for $\mathrm{M}_2/\mathrm{M}_4$. The evolution of $\overline{\varepsilon}$ as a function of h/A_{M_2} is shown in Fig. 9. It becomes clear from this Figure, that there is no linear relationship between $\overline{\varepsilon}$ and ε. A maximum seems to be reached around $h/A_{\mathrm{M}_2} = 25$, which is close to the resonance depth. More important, low values high values of $\overline{\varepsilon}$ do not necessarily coincide with large values of h/A_{M_2}. Since the relationship between the norm of the difference between iFlow and Telemac

Figure 9 – Evolution of the estuary averaged ε as a function of ε.

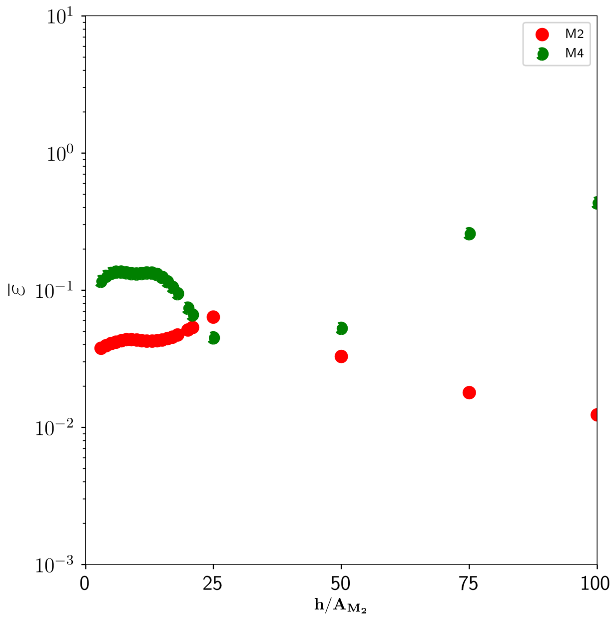

and h/A_{M_2} appears weak, it is interesting to investigate if the relationship between the norm of the difference between iFlow and Telemac and $|\varepsilon|$ is more pronounced. As a result, the norm of the difference between iFlow and Telemac is displayed in Fig. 10. However, such a relationship does not appear clearly. These results imply that the differences between iFlow and Telemac can not be estimated via a single parameter h/A_{M_2} or $|\varepsilon|$, but are governed by a more complex interplay between water-depth, resonance and friction.

Figure 10 – Difference between iFlow and Telemac as a function of the estuary averaged ε.

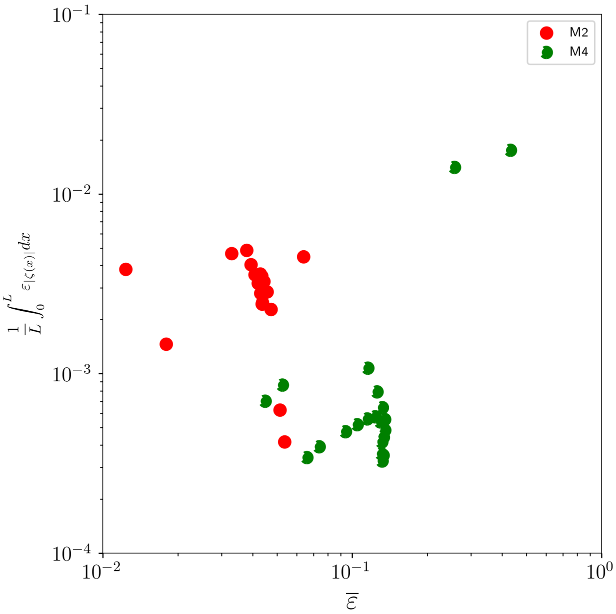

5.5 Conclusion

Based on the results shown in the present report, we can draw the following conclusions:

- In the tested configuration, it was not possible to determine a ratio of h/A_{M_2} at which iFlow clearly fails at reproducing the results of Telemac
- No single parameter governing the differences between iFlow and Telemac has been identified

Furthermore, we suggest that any follow up study should tackle the following challenges

- More data (i.e. number of simulations) is required to carry out a significant study about the differences between iFlow and Telemac
- iFlow needs to be pushed to the limits in terms of h/A_{M_2} ratio but also in terms of the average ratio h/A_{M_2} (i.e., $\overline{\varepsilon}$)
- A method to overcome or at least reduce the transient period in Telemac is necessary to shorten computational time and to limit data output from a single Telemac simulation

The results of iFlow and Telemac for the present configuration agree very well. However, due to the choices for the parameter values, the models have not yet been thouroughly challenged. Indeed, it was chosen to vary the A_{M_2}/H by keeping A_{M_2} constant and varying H. This method allow to maintain the same value of A_{M_4}/AMt for all the simulations. However, by varying H, we also varied the amount of friction, which caused the tidal wave to be rapidly damped for low value of A_{M_2}/H. These were the value for which the largest difference between the Telemac and iFlow were expected, but due to the damping, the hypothesis $A_{\mathrm{M}_2}/H \ll 1$ was still valid in the upper estuary. In the lower estuary, this hypothesis was challenged, but the water-level was imposed at the seaward boundary. As a result, the expected differences between iFlow and Telemac did not occur.

In a follow-up study, it is strongly adviced to vary the A_{M_2}/H by keeping H constant and vary both A_{M_2} and A_{M_4} simultaneously such that $A_{\mathrm{M}_4}/A_{\mathrm{M}_2}$ remains constant. In this way, only the A_{M_2}/H ratio varies, like in the present study, but friction should not affect the outcome of the comparison. The present plots, displaying the difference between iFlow and Telemac as a function of A_{M_2}/H could then be reproduced. The convergence of the Telemac simulation can subsequently be checked by repeating the graphs using the Telemac results after a different number of oscillations. These results could be compared to Telemac results for which the initial condition are the iFlow results, to see if the convergence time decreases. The convergence criterium should be based on the difference in value between two successive periods, compared to the local value of ε.

To finish the procedure should be reiterated by varying H, keeping both A_{M_2}/H and $A_{\mathrm{M}_4}/A_{\mathrm{M}_2}$ constant. It is recomended to focus on parameter values lying in different regimes, e.g. a value of H for which strong damping occurs, and a value of H for which resonance occurs.

References

Bi, **Q.; Kaptein**, **S.; Schramkowski**, **G.; Smolders**, **S.; Mostaert**, **F.** (2020). The iFlow inspired TELEMAC-3D model. Sub report 1 – Comparing ETM dynamics with the iFlow model. *WL Rapporten*, WL2020R19_025_1. Flanders Hydraulics Research: Antwerp, Belgium

Brouwer, **R. L.; Schramkowski**, **G. P.; Dijkstra**, **Y. M.; Schuttelaars**, **H. M.** (2018). Time Evolution of Estuarine Turbidity Maxima in Well-Mixed, Tidally Dominated Estuaries: The Role of Availability-and Erosion-Limited Conditions. *Journal of Physical Oceanography 48 (8)*: 1629–1650

Brouwer, **T.; Schramkowski**, **G.; Mostaert**, **F.** (2017). Geïdealiseerde processtudie van systeemovergangen naar hypertroebelheid. 2.0. *WL Rapporten*, 13_103_3. Flanders Hydraulics Research: Antwerp, Belgium

Dijkstra, **Y. M.** (2017). *iFlow modelling framework. User manual & technical description.*

Dijkstra, **Y. M.; Brouwer**, **R. L.; Schuttelaars**, **H. M.; Schramkowski**, **G. P.** (2017). The iFlow modelling framework v2. 4: a modular idealized process-based model for flow and transport in estuaries. *Geoscientific Model Development 10 (7)*: 2691–2713

Dijkstra, **Y. M.; Schuttelaars**, **H. M.; Schramkowski**, **G. P.** (2019a). A Regime Shift From Low to High Sediment Concentrations in a Tide-Dominated Estuary. *Geophysical Research Letters 46 (8)*: 4338–4345

Dijkstra, **Y. M.; Schuttelaars**, **H. M.; Schramkowski**, **G. P.; Brouwer**, **R. L.** (2019b). Modeling the Transition to High Sediment Concentrations as a Response to Channel Deepening in the Ems River Estuary. *124 (3)*: 1578–1594

Malcherek, **A.** (2000). Application of TELEMAC-2D in a narrow estuarine tributary. *14 (13)*: 2293–2300

Smolders, **S.; Maximova**, **T.; Vanlede**, **J.; Plancke**, **Y.; Verwaest**, **T.; Mostaert**, **F.** (2016). Integraal Plan Bovenzeeschelde: Subreport 1 – SCALDIS: a 3D Hydrodynamic Model for the Scheldt Estuary. 5.0. *WL Rapporten*, 13_131. Flanders Hydraulics Research: Antwerp, Belgium

DEPARTMENT **MOBILITY & PUBLIC WORKS**
Flanders hydraulics Research

Berchemlei 115, 2140 Antwerp
T +32 (0)3 224 60 35
F +32 (0)3 224 60 36
waterbouwkundiglabo@vlaanderen.be
www.flandershydraulicsresearch.be